Article | Received 15 September 2026; Revised 29 October 2026; Accepted 4 November 2026; Published 18 November 2026
https://doi.org/10.55092/aimat20260015

Supplementary data

Unraveling intermediate–active site interaction mechanisms for tuning CO_2 reduction selectivity via ML-DFT

Tianxiang Li[1], Yikai Yu[1], Hao Ren[1], Houyu Zhu[1], Wen Zhao[1], Yuhua Chi[1,*], Yong Liu[2] and Wenyue Guo[1]

[1] School of Materials Science and Engineering, Shandong Key Laboratory of Intelligent Energy Materials, China University of Petroleum (East China), Qingdao, China
[2] Department of Chemistry, University of Colorado Denver, Denver, USA

* Correspondence author; E-mail: chiyuhua@upc.edu.cn.

1. Supplementary tables

Table S1. Gibbs free energy changes of elementary reaction steps during CO_2 reduction on M@N-WS_2 catalysts.

	Rh@N-WS_2	Pd@N-WS_2	Ir@N-WS_2	Pt@N-WS_2
ΔG(*CO_2 → *COOH) (eV)	−0.16723	−0.01729	−0.50647	−0.43932
ΔG(*CO_2→*HCOO) (eV)	0.04592	0.62157	0.57029	0.27115
ΔG(*COOH→*CO) (eV)	−0.15140	−0.43543	−0.98761	−0.7815
ΔG(*COOH→*HCOOH) (eV)	0.00774	0.21915	0.27810	−0.37498
ΔG(*CO→*CHO) (eV)	0.18235	0.23698	1.31196	0.78370
ΔG(*CO→*COH) (eV)	0.60593	1.41780	1.65891	1.03051
ΔG(*CHO→*CHOH) (eV)	−0.03199	0.74626	−0.32397	0.09564
ΔG(*CHO→*CH_2O) (eV)	0.66552	0.80836	−0.14773	1.03519
ΔG(*CHOH→*CH_2OH) (eV)	0.26984	−0.5905	0.57876	−0.0898
ΔG(*CHOH→*CH (eV)	1.50499	1.0344	1.13885	0.75526
ΔG(*CH_2OH→*CH_3OH) (eV)	−0.24222	0.22123	0.15670	0.47419
ΔG(*CH_2OH→*CH_2) (eV)	0.33029	0.95613	−0.09933	0.29908
ΔG(*CH_2→*CH_3) (eV)			−0.77486	−0.94585
ΔG(*CH_3→*CH_4) (eV)			−0.01143	0.10105

Copyright©2026 by the authors. Published by ELSP. This work is licensed under Creative Commons Attribution 4.0 International License, which permits unrestricted use, distribution, and reproduction in any medium provided the original work is properly cited.

Table S2. Detailed information on the eleven original descriptors, classified into three categories. loaded-atom-related, catalyst-related, and reactant-related descriptors.

Category	Name	Abbreviation
Load atom part	Atomic radius of X	r_{m_X}
	Atomic number of X	Z_X
	Atomic mass of X	M_X
	Electronegativity	χ_X
	First ionization energy	IE_1
	d electron number of X	N_d
Catalyst part	d-band center	ε_d
	Work function	σ
Reactant part	Adsorption energy of initial-state intermediate	E_{adsIS}
	Adsorption energy of final-state intermediate	E_{adsFS}
	Integrated crystal orbital Hamilton population	ICOHP

Table S3. Mathematical operators used in SISSO.

Mathematical operators	Description
+	Addition
-	Subtraction
*	Multiplication
/	Division
^2	Square
^3	Cube
sqrt	Square root
|-|	Absolute value

Table S4. Numerical values of the primary features used for SISSO modeling of reaction free-energy changes on Rh@N-WS_2.

	Rh_1	Rh_2	Rh_3	Rh_4	Rh_5	Rh_6
ΔG(eV)	−0.167	−0.151	0.182	−0.031	0.269	−0.242
E_{adsIS} (eV)	−0.349	−2.955	−1.681	−2.979	−3.553	−2.461
E_{adsFS} (eV)	−2.955	−1.681	−2.979	−3.553	−2.461	−0.589
ICOHP (eV)	−2.435	−3.819	−4.916	−4.148	−4.644	−2.864
σ (eV)	5.026	5.026	5.026	5.026	5.026	5.026
ε_d (eV)	−1.706	−1.706	−1.706	−1.706	−1.706	−1.706
IE_1 (eV)	7.460	7.460	7.460	7.460	7.460	7.460
N_d	8.000	8.000	8.000	8.000	8.000	8.000
χ_X	2.280	2.280	2.280	2.280	2.280	2.280

Table S5. Numerical values of the primary features used for SISSO modeling of reaction free-energy changes on Pd@N-WS_2.

	Pd_1	**Pd_2**	**Pd_3**	**Pd_4**	**Pd_5**	**Pd_6**
ΔG(eV)	−0.017	−0.435	0.236	0.746	−0.590	0.221
E_{adsIS} (eV)	−0.224	−2.849	−1.887	−3.094	−2.902	−2.670
E_{adsFS} (eV)	−2.849	−1.887	−3.094	−2.902	−2.670	−0.415
ICOHP (eV)	−2.062	−3.240	−4.299	−3.855	−3.859	−2.721
σ (eV)	5.113	5.113	5.113	5.113	5.113	5.113
ε_d (eV)	−1.971	−1.971	−1.971	−1.971	−1.971	−1.971
IE_1 (eV)	8.340	8.340	8.340	8.340	8.340	8.340
N_d	10.000	10.000	10.000	10.000	10.000	10.000
χ_X	2.200	2.200	2.200	2.200	2.200	2.200

Table S6. Numerical values of the primary features used for SISSO modeling of reaction free-energy changes on Ir@N-WS_2.

	Ir_1	**Ir_2**	**Ir_3**	**Ir_4**	**Ir_5**	**Ir_6**
ΔG(eV)	−0.506	−0.987	1.311	−0.323	0.578	−0.099
E_{adsIS} (eV)	−0.657	−3.586	−3.176	−3.419	−4.234	−2.910
E_{adsFS} (eV)	−3.586	−3.176	−3.419	−4.234	−2.910	−5.232
ICOHP (eV)	−3.030	−4.154	−5.698	−4.292	−5.045	−3.174
σ (eV)	5.026	5.026	5.026	5.026	5.026	5.026
ε_d (eV)	−1.994	−1.994	−1.994	−1.994	−1.994	−1.994
IE_1 (eV)	9.100	9.100	9.100	9.100	9.100	9.100
N_d	7.000	7.000	7.000	7.000	7.000	7.000
χ_X	2.200	2.200	2.200	2.200	2.200	2.200

Table S7. Numerical values of the primary features used for SISSO modeling of reaction free-energy changes on Pt@N-WS_2.

	Pt_1	**Pt_2**	**Pt_3**	**Pt_4**	**Pt_5**	**Pt_6**
ΔG(eV)	−0.439	−0.781	0.783	0.095	−0.089	0.299
E_{adsIS} (eV)	−0.435	−3.480	−2.785	−3.598	−4.092	−3.321
E_{adsFS} (eV)	−3.480	−2.785	−3.598	−4.092	−3.321	−5.092
ICOHP (eV)	−2.679	−3.900	−5.344	−4.266	−4.632	−3.457
σ (eV)	5.064	5.064	5.064	5.064	5.064	5.064
ε_d (eV)	−2.160	−2.160	−2.160	−2.160	−2.160	−2.160
IE_1 (eV)	9.000	9.000	9.000	9.000	9.000	9.000
N_d	9.000	9.000	9.000	9.000	9.000	9.000
χ_X	2.280	2.280	2.280	2.280	2.280	2.280

Table S8. Training and test sample assignments for leave-one-metal-out cross-validation.

CV fold	Test-set metal	Training samples	Test samples
CV_1	Rh	Pd1–Pd6, Ir1–Ir6, Pt1–Pt6	Rh1–Rh6
CV_2	Pd	Rh1–Rh6, Ir1–Ir6, Pt1–Pt6	Pd1–Pd6
CV_3	Ir	Rh1–Rh6, Pd1–Pd6, Pt1–Pt6	Ir1–Ir6
CV_4	Pt	Rh1–Rh6, Pd1–Pd6, Ir1–Ir6	Pt1–Pt6

Table S9. Changes in test-set RMSE (ΔRMSE, in eV) upon removal of each primary feature.

ΔRMSE (eV)	CV_1	CV_2	CV_3	CV_4
E_{adsIS} (eV)	0.00179	0.05926	0.00604	0.02200
E_{adsFS} (eV)	0.01948	0.08935	0.00924	0.06267
ICOHP (eV)	0.03775	0.10612	0.02197	0.07236
σ(eV)	0.02086	0.05481	0.00399	0.00338
ε_d (eV)	0.00757	0.07391	0.01484	0.02033
IE_1 (eV)	0.00176	0.04922	0.00440	0.00635
N_d	0.01891	0.07270	0.01330	0.04587
χ_X	0.00498	0.05489	0.00440	0.06513

2. Supplementary figures

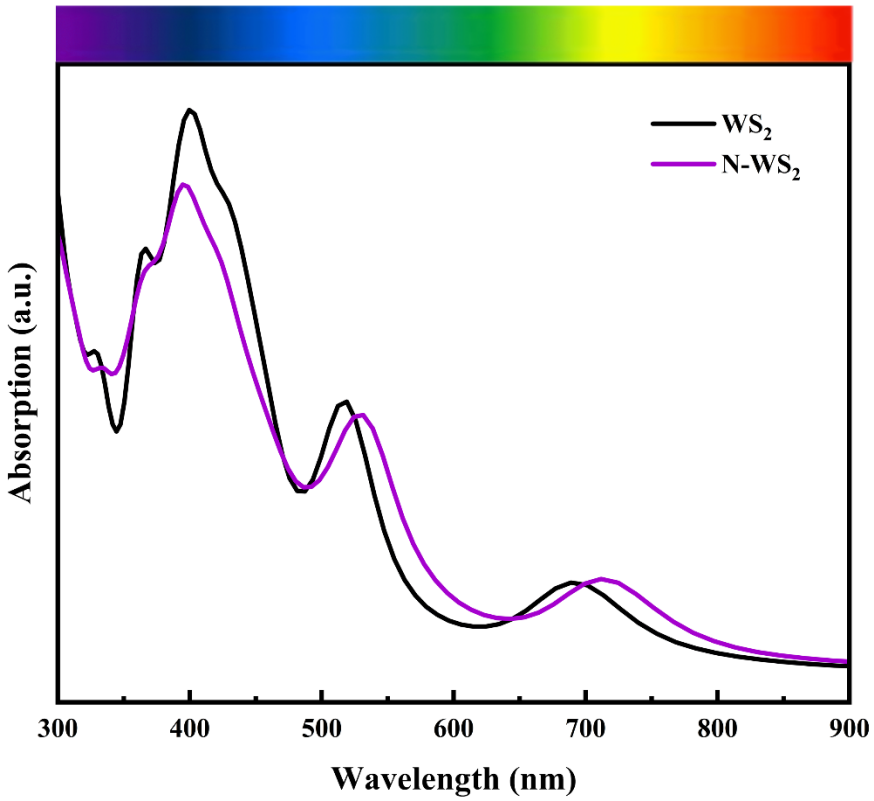


Figure S1. Calculated optical absorption spectra of pristine WS_2 and N-WS_2.

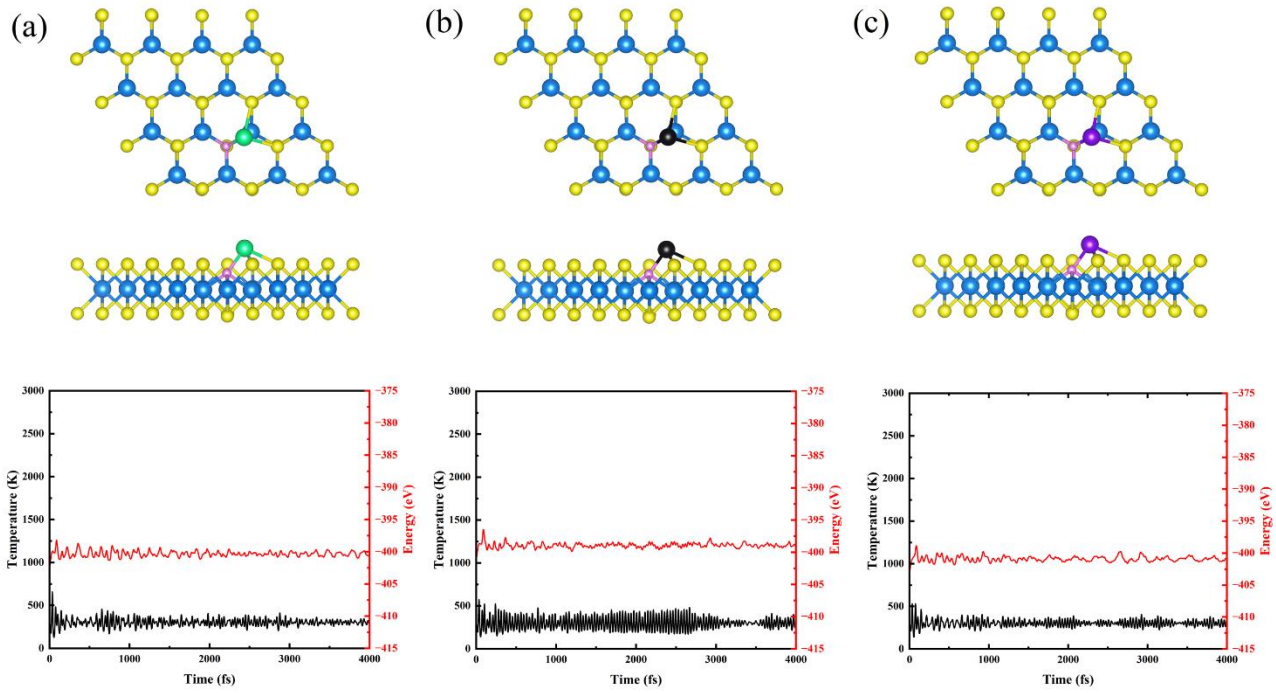


Figure S2. Top and side views of the most stable geometric configurations of **(a)** Rh@N-WS_2; **(b)** Pd@N-WS_2; and **(c)** Ir@N-WS_2. The corresponding AIMD results show the energy evolution (red line, right axis) and temperature variation (black line, left axis) during the 4 ps simulation at 300 K with a time step of 1 fs.

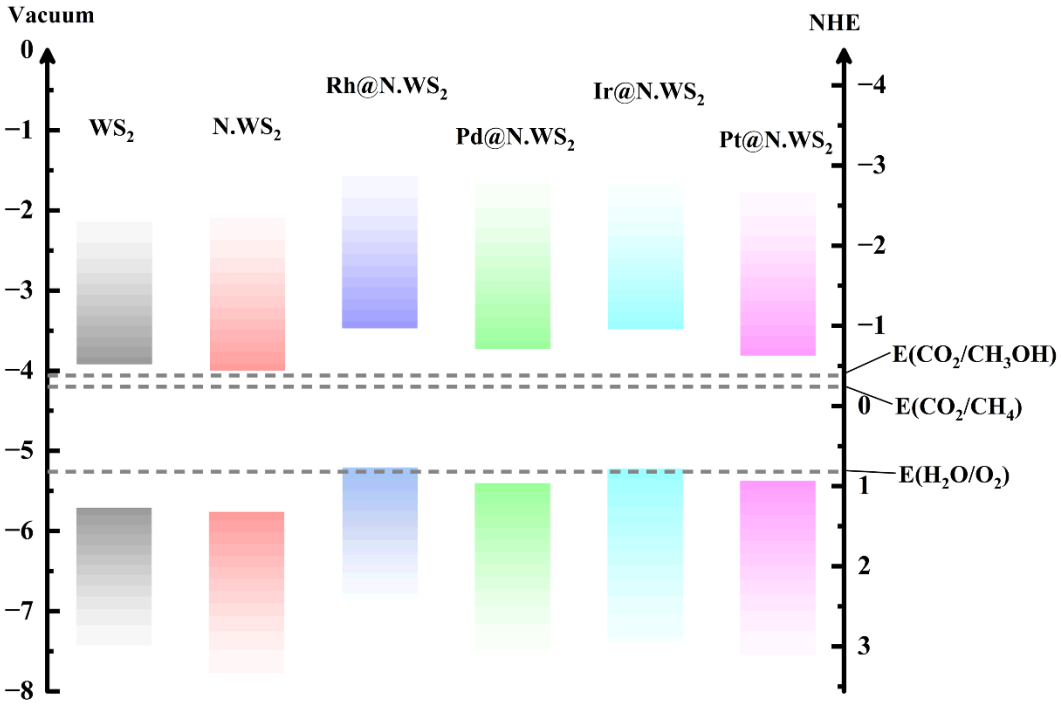


Figure S3. Band-edge alignment referenced to the vacuum level and the normal hydrogen electrode (NHE).

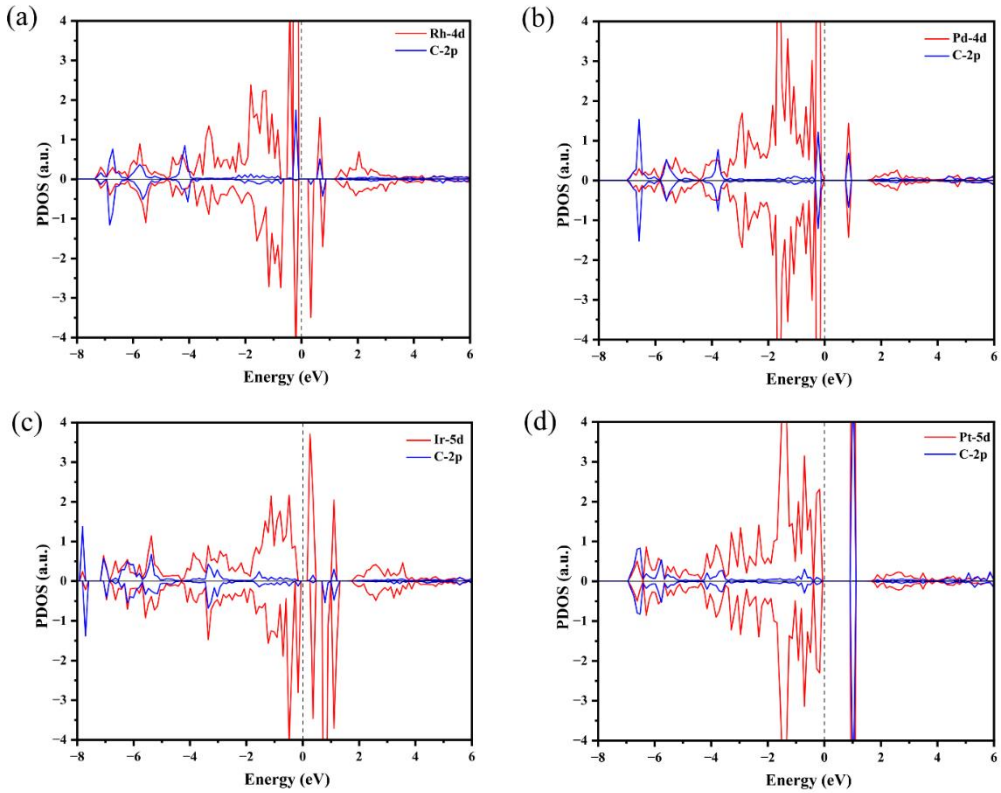


Figure S4. Projected density of states (PDOS) of the M-d and C-p orbitals for *CH_2OH adsorbed on **(a)** Rh@N-WS_2; **(b)** Pd@N-WS_2; **(c)** Ir@N-WS_2; and **(d)** Pt@N-WS_2.

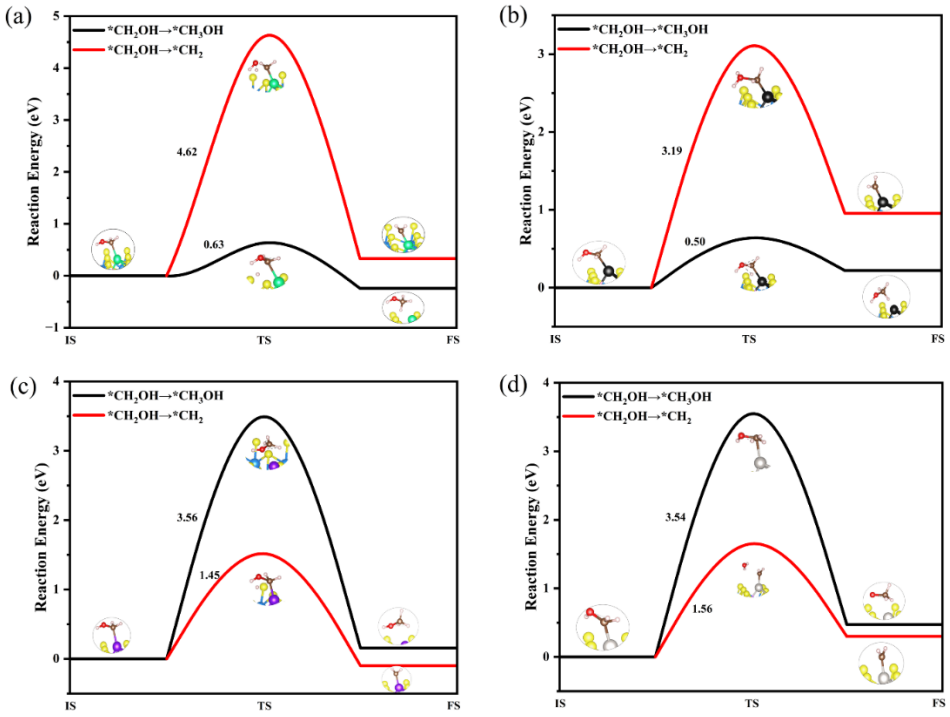


Figure S5. Reaction energy profiles for the competing conversions of *CH_2OH to *CH_3OH (black) and *CH_2 (red) on **(a)** Rh@N-WS_2; **(b)** Pd@N-WS_2; **(c)** Ir@N-WS_2; and **(d)** Pt@N-WS_2. Insets show the initial (IS), transition (TS), and final (FS) structures. The labeled values indicate activation energy barriers in eV.

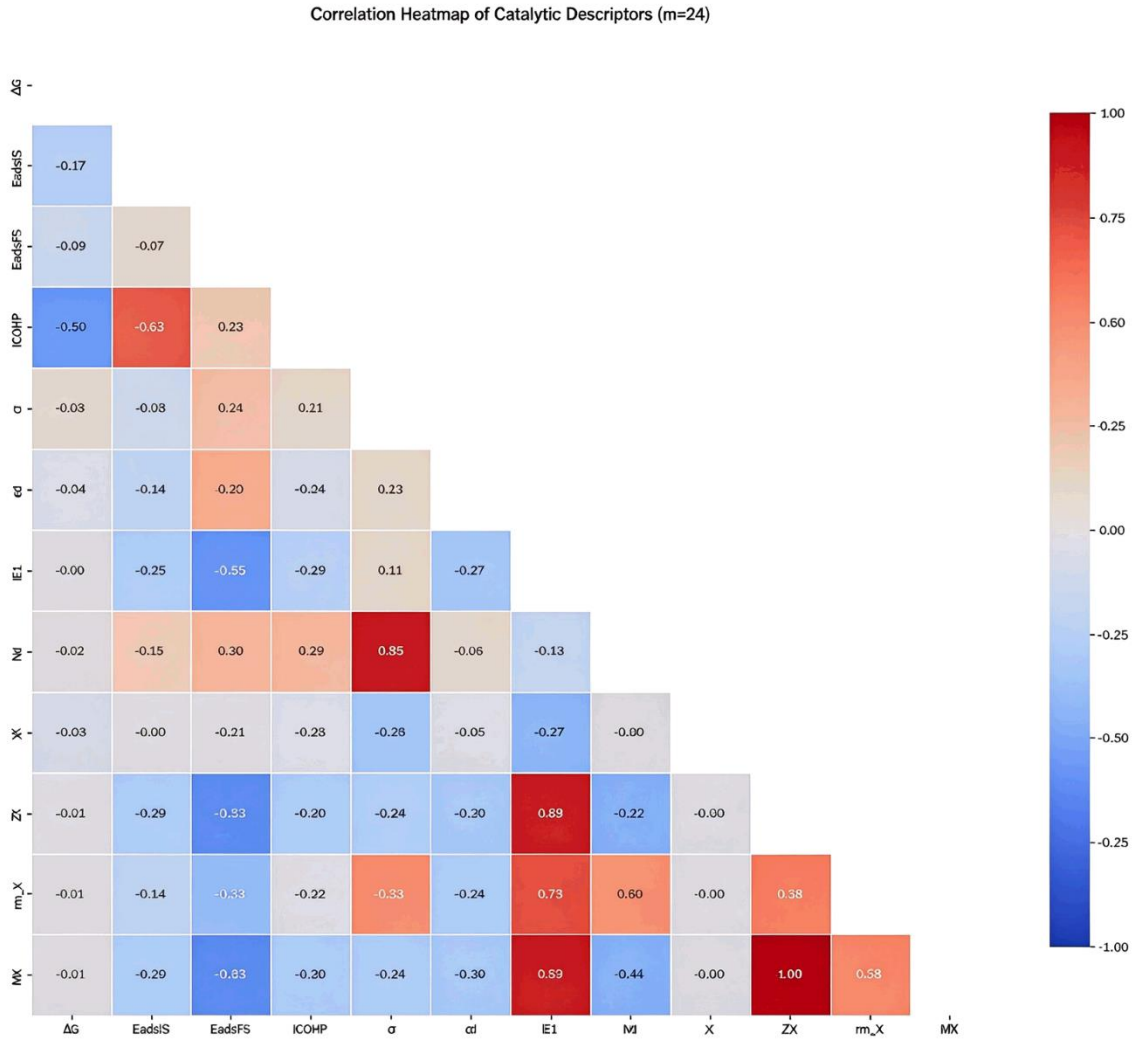


Figure S6. Heatmap of pairwise correlations between energy-related properties and different descriptors.

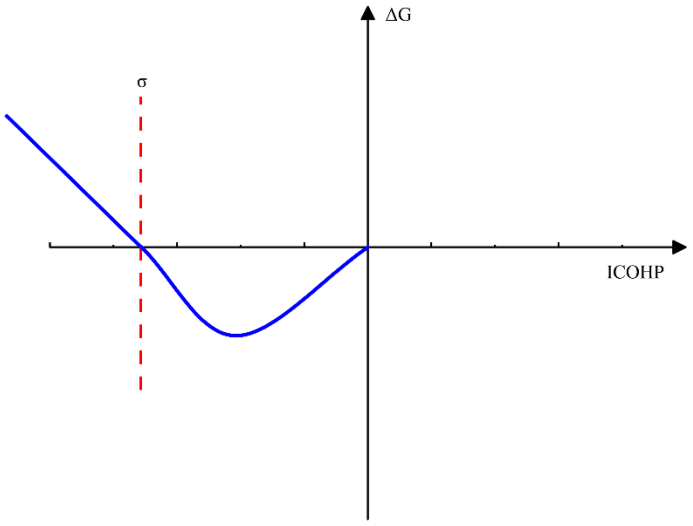


Figure S7. Schematic curve showing the nonlinear relationship between ICOHP and the ΔG_{Pred}. The red dashed line denotes a characteristic ICOHP point (σ).

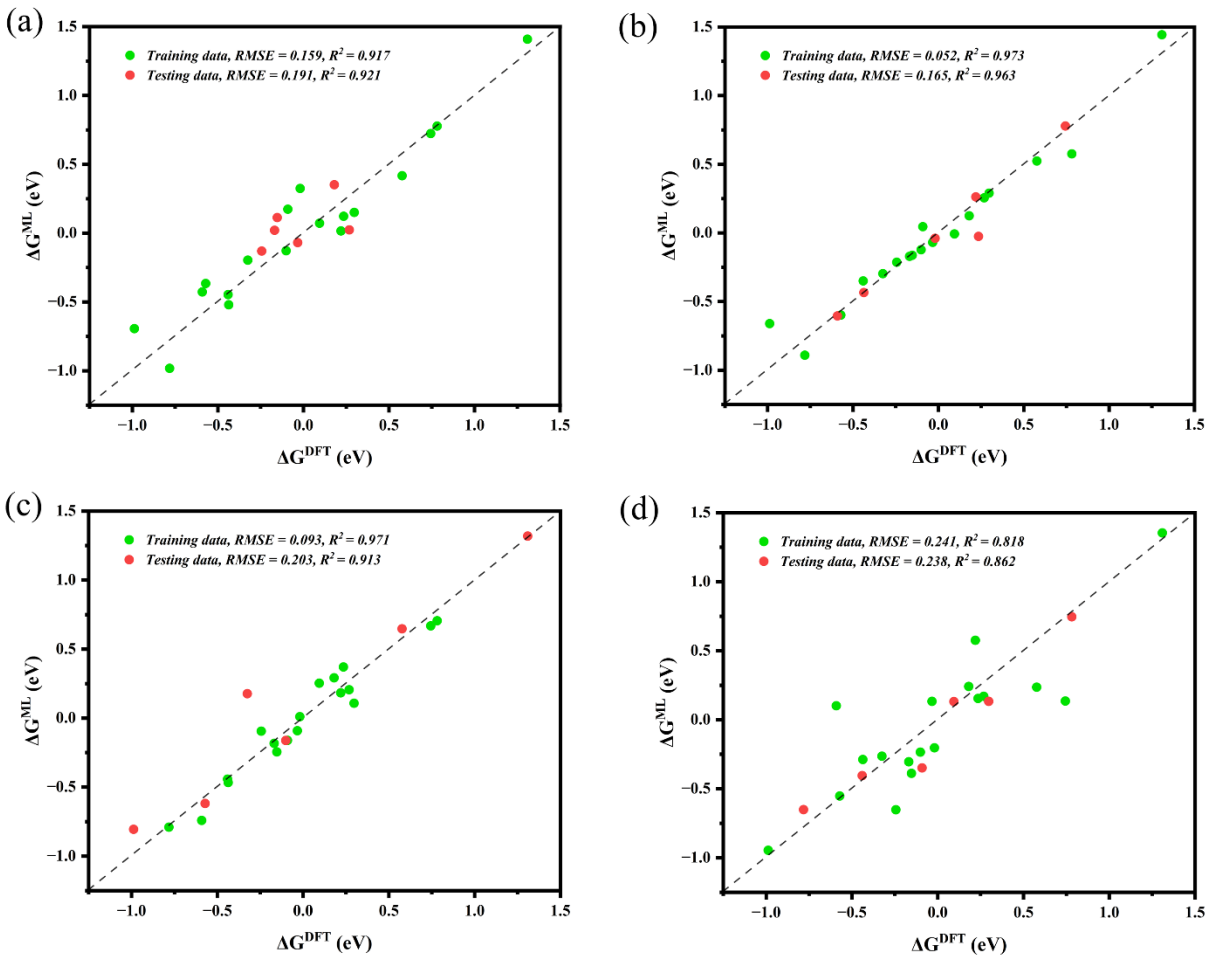


Figure S8. Comparison of SISSO-predicted and DFT-calculated ΔG values for the training and held-out test sets in leave-one-metal-out cross-validation. **(a)** CV_1; **(b)** CV_2; **(c)** CV_3; and **(d)** CV_4. The corresponding R^2 and RMSE values are shown in each panel; RMSE is reported in eV.